PAPER

Check for updates

Thermal gradient-driven heavy metal speciation and risk evolution in municipal and industrial sludge: a 300–700 °C pyrolysis perspective

Ke Zhao, [abc] Chundi Si,*[ab] Pei Zhang[c] and Yaning Cui[ab]

This work investigated the effect of pyrolysis temperatures (300–700 °C) on the speciation distribution and environmental risks of heavy metals (Cu, Zn, Pb, Cd, Ni, Cr) in biochar derived from municipal sludge (MS) and industrial sludge (IS). Through analyses of characterization, heavy metal content, sequential extraction experiment, leaching experiments, and ecological risk assessment, high-temperature pyrolysis promoted the migration of heavy metals into stable forms. The stabilization mechanism primarily relied on the increased specific surface area and porosity of biochar, leading to surface adsorption and pore-filling effects. In contrast, the stabilization of Cu and Ni under low-temperature pyrolysis was closely associated with complexation involving N/O-containing functional groups. The leaching concentration of heavy metals in pyrolytic biochar exhibited a gradual decrease with increasing pyrolysis temperature, and the potential ecological risk index decreased compared to raw sludge. The results demonstrated that high-temperature pyrolysis technology can effectively achieve the stabilization and resource recovery of heavy metals in sludge.

1 Introduction

In recent years, with the increasing number and scale of wastewater treatment plants in China, the discharge of residual sludge has continued to rise.[1] In 2015, the municipal sludge output in China reached 35 million tons, and it is projected to increase to 60–90 million tons by 2020.[2] The composition of sludge from urban wastewater treatment plants is highly diverse, potentially containing large quantities of pathogens, inorganic or organic toxic pollutants (such as trace metals and polycyclic aromatic hydrocarbons), which exhibit characteristics of high toxicity, long latency periods, and a tendency to accumulate in the food chain.[1,3] For example, the accumulation of the heavy metal copper (Cu) in the human body can disrupt cerebral copper metabolism and accelerate the progression of Alzheimer's and Parkinson's diseases.[4,5] Therefore, the harmless treatment of sludge is of utmost importance. Currently, the primary disposal methods for residual sludge in China include landfilling, composting, natural drying, and incineration.[6,7] Among these techniques, landfilling and composting may severely contaminate groundwater and soil; natural drying fails to effectively remove hazardous substances from sludge; and incineration generates large amounts of harmful gases,

polluting the environment.[8] Pyrolysis is a widely applied solid waste treatment technology that decomposes organic materials under oxygen-free conditions into liquid, solid, and volatile products.[9] It can effectively degrade organic pollutants in sludge, sterilize pathogens, immobilize heavy metals, and achieve volume reduction.

In recent years, sludge biochar with high stability, tunable porous structure, and easy surface modification has been employed for the removal of various pollutants.[10–12] However, studies have shown that the majority of heavy metals in sludge remain in the biochar after pyrolysis, limiting its further application.[6,13] Devi *et al.*[14] found that biochar derived from paper mill sludge is rich in heavy metals, primarily Cd, Cr, Cu, Ni, Pb, and Zn. The migration behavior of heavy metals during pyrolysis and found that the alkalinity of biochar enhances the immobilization of endogenous heavy metals, thereby reducing their environmental risks during application.[15] In terms of environmental effect assessment, total metal content can indicate the overall levels and mobility of metals in sludge. However, the bioavailability and associated ecotoxicity of heavy metals largely depend on their specific chemical forms or binding states.[16] To effectively determine metal speciation, the Bureau Community of Reference (BCR) proposed a three-step sequential extraction method, which classifies extracted metal forms into four categories: (1) exchangeable and carbonate-bound fractions, referred to as bioavailable forms; (2) reducible forms; (3) organic and sulfide-bound forms, referred to as oxidizable forms; and (4) silicate lattice or crystalline forms, referred to as residual forms.[3,9,15] Among these, the residual

[a] School of Traffic and Transportation, Shijiazhuang Tiedao University, Shijiazhuang, Hebei Province 050043, China. E-mail: sichundi@stdu.edu.cn

[b] Hebei Key Laboratory of Traffic Safety and Control, Shijiazhuang, Hebei Province 050043, China

[c] Shijiazhuang University, Shijiazhuang, Hebei Province 050035, China

fraction of heavy metals is stable and exhibits low environmental toxicity, while the acid-extractable and reducible fractions are unstable and pose higher environmental risks.[1] Studies have found that the speciation of heavy metals undergoes transformation during sludge pyrolysis, promoting the conversion of unstable forms into more stable ones.[8,14,15] Ji et al.[9] demonstrated that increasing pyrolysis temperature facilitates metal stabilization, with significant decreases in the percentages of acid-extractable and reducible fractions and notable increases in oxidizable and residual fractions, which predominantly exist in biochar. Li et al.[7] also confirmed that during sludge pyrolysis, a substantial portion of heavy metals can migrate from bioavailable fractions to more stable fractions.

This study systematically investigates the migration patterns, speciation distribution characteristics, and dominant stabilization mechanisms of Cd, Cu, Cr, Ni, Zn, and Pb at different pyrolysis temperatures (300–700 °C) using municipal sludge (MS) and industrial sludge (IS) as subjects. By integrating physicochemical characterization, sequential extraction, and leaching experiments, the study quantitatively analyzes the transformation pathways of heavy metals. Furthermore, risk assessment indices and potential ecological risk indices are employed to evaluate the ecotoxicity of sludge-derived biochar for resource utilization. The research aims to clarify the regulatory role of pyrolysis temperature on the environmental behavior of heavy metals, providing multidimensional theoretical support for the safe resource utilization of sludge.

2 Materials and methods

2.1 Determination of heavy metal content

Approximately 0.1 g of the sample was accurately weighed and placed in a polytetrafluoroethylene digestion vessel. Then, 10 mL of HCl was added for pre-digestion for over 10 h. Subsequently, 5 mL of HNO_3, 5 mL of HF, and 2 mL of $HClO_4$ were added. The vessel was sealed and heated on an electric hotplate at 110 °C for 1.5–2 h. After removing the lid to expel yellow fumes, the temperature was raised to 130 °C until the solution evaporated to approximately 1 mL. Upon cooling to room temperature, 1 mL of 50% HNO_3 solution was added, and the mixture was transferred to a 50 mL colorimetric tube for volume adjustment. The solution was filtered through a 0.22 μm nylon membrane, and the concentrations of Zn, Cr, Cu, Pb, Ni, and Cd in the filtrate were determined using Inductively Coupled Plasma Mass Spectrometry (ICP-MS, Shimadzu ICPE-9000, Japan).

2.1.1 Sequential extraction experiment. A modified sequential extraction method proposed by the European Communities Bureau of Reference (BCR) was employed for the sequential extraction of heavy metals in sludge and biochar.[9,15] According to this method (Table 1), heavy metal speciation was classified into three categories: (1) bioavailable fraction (F1) and reducible fraction (F2): these fractions exhibit high bioavailability or direct ecotoxicity; (2) oxidizable fraction (F3): this fraction has potential bioavailability and can be leached under highly acidic or oxidizing conditions; (3) residual fraction (F4):

Table 1 The BCR three-step sequential extraction method

Step	Speciation	Method
I	Bioavailable fraction (F1)	Briefly, 0.50 g of sample was placed into a plastic centrifuge tube, followed by the addition of 30 mL of 0.11 mol L^{-1} acetic acid solution. The mixture was shaken on a rotary shaker for 16 h and then centrifuged at 3000 r min^{-1}. The supernatant was collected, filtered through a 0.45 μm membrane, diluted, and subsequently analyzed. The remaining residue was washed by adding 20 mL of deionized water, shaking for 20 min, and centrifuging to remove the supernatant, in order to eliminate residual acetic acid from the solid fraction prior to the next extraction step
II	Reducible fraction (F2)	The residue obtained from step I was treated with 30 mL of 0.1 mol L^{-1} NH_2OH HCl solution, and the subsequent procedures were carried out in the same manner as in step I
III	Oxidizable fraction (F3)	The residue obtained from step II was treated with 6 mL of 8.8 mol L^{-1} H_2O_2 solution and left to stand at room temperature for 1 h. It was then subjected to a water bath at (85 ± 2) °C until evaporation was complete. After cooling to room temperature, 30 mL of 1.0 mol L^{-1} NH_4Ac solution (pH = 2) was added, and the subsequent procedures were carried out in the same manner as in step I
IV	Residual fraction (F4)	Subtraction method

this fraction is non-bioavailable, resistant to leaching or degradation, and considered to have negligible ecotoxicity or bioavailability.

2.1.2 Leaching experiment. The toxicity characteristic leaching procedure (TCLP), recommended by the U.S. Environmental Protection Agency (EPA), was used to determine leaching concentrations.[9] An extraction solution (pH 2.88 ± 0.05) was prepared using glacial acetic acid. A liquid-to-solid ratio of 20 : 1 was maintained, and the mixture was shaken at 200 rpm for 18 ± 2 h at 25 °C. After centrifugation and filtration, the heavy metal concentrations in the filtrate were measured.

2.1.3 Heavy metal risk assessment methods. The descriptions of the risk assessment index and the potential ecological risk Index were provided in the SI.

3 Results and discussion

3.1 Characterization of biochar

3.1.1 Surface morphology analysis. The surfaces (Fig. 1) of both raw sludge types exhibited an uneven texture. The municipal sludge (MS) displayed relatively underdeveloped pore structures, while the industrial sludge (IS) featured more pronounced grooves. As pyrolysis temperature increased, both sludge types gradually fragmented into smaller particulate structures.

The pH (Table 2) of MS was 6.85, and that of IS was 6.97, both weakly acidic. When pyrolysis temperature rose to 700 °C, the pH of MS and IS pyrolysis products increased to 8.45 and 9.52, respectively. This alkalization phenomenon was closely associated with the formation of alkaline substances (e.g., metal oxides, carbonates, or alkaline ash) during high-temperature pyrolysis. Notably, IS exhibited a more significant pH increase, likely due to its higher content of precursors (e.g., calcium and magnesium salts) convertible to alkaline compounds.[17] The elevated pH promoted the precipitation of some heavy metals as hydroxides, which further decomposed into metal oxides during pyrolysis, enhancing heavy metal stabilization.[2]

Ash content (Table 2) showed a monotonic increase with rising pyrolysis temperature. For MS, ash content increased from 56.74% in raw sludge to 75.42% at 700 °C, while IS ash content rose from 64.73% to 81.43%. This trend reflected the volatilization and decomposition of organic components during pyrolysis, resulting in the relative enrichment of inorganic residues (e.g., silicates, metal oxides).[18] Notably, IS consistently exhibited higher ash content than MS across all temperatures, suggesting either higher initial inorganic content. These differences may stem from sludge sources (e.g., industrial sludge containing more inorganic additives).[19]

3.1.2 Elemental composition. With increasing pyrolysis temperature, the contents (Table 2) of C, H, N, S, and O in sludge gradually decreased. For MS, C content dropped from 23.69% to 14.06% at 700 °C, while IS decreased from 19.86% to 12.26%. C loss primarily resulted from the cracking of aliphatic and aromatic organic compounds into gaseous products (e.g., CO, CO_2, or CH_4).[9] H reduction indicated intensified dehydrogenation and aromatization reactions, while rapid O loss was directly linked to the thermal removal of oxygen-containing functional groups.[20] Declines in N and S were attributed to the thermal decomposition of proteins and sulfur-containing compounds, releasing gases such as NH_3 and SO_2.[3,21] The H/C ratios of MS and IS decreased from 0.073 and 0.083 to 0.042 and 0.051, respectively, at 700 °C, signifying enhanced carbon skeleton aromatization and the conversion of aliphatic structures into polycyclic aromatic hydrocarbons.[15,16] IS consistently exhibited lower H/C ratios than MS, indicating higher aromatization degrees in its pyrolysis products.

3.1.3 Porosity and surface properties. In Table 2, the specific surface area (SSA) of MS increased dramatically from 12.87 m^2 g^{-1} to 105.34 m^2 g^{-1} at 700 °C, whereas IS only rose from 5.69 m^2 g^{-1} to 48.46 m^2 g^{-1}. The high SSA of MS-derived biochar originated from microporous structures formed via intense volatile release at high temperatures, while IS's lower values likely resulted from pore blockage caused by its high ash content (81.43%). Pore volume (PV) expanded from 0.023 cm^3 g^{-1} to 0.371 cm^3 g^{-1} for MS and from 0.008 cm^3 g^{-1} to 0.103 cm^3 g^{-1} for IS, suggesting that MS pyrolysis favored the development of interconnected hierarchical pore structures.[18] The average pore diameters (PD) of both sludge types initially increased before decreasing, peaking at 300 °C (12.92 nm for MS; 10.49 nm for IS). At 700 °C, average pore diameters reduced to 3.61 nm (MS) and 5.40 nm (IS), with differences potentially
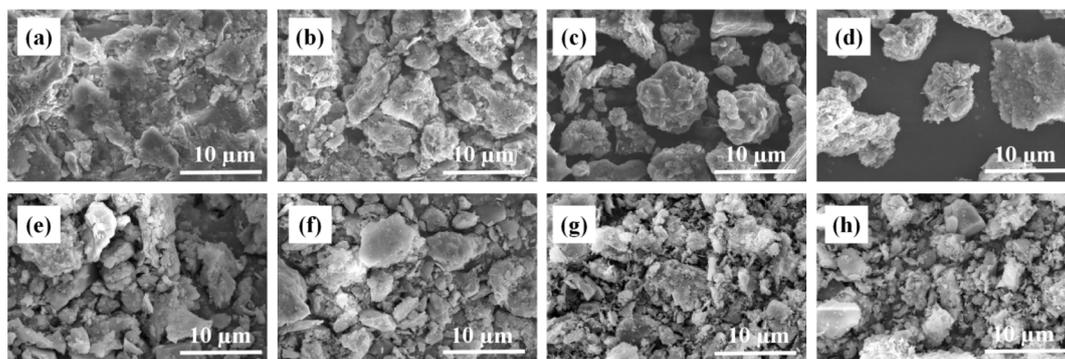

Fig. 1 Morphology of sludge and its pyrolysis products ((a): MS, (b): MS300, (c): MS500, (d): MS700, (e): IS, (f): IS300, (g): IS500, (h): IS700).

Table 2 Analysis of physicochemical properties of different types of sludge and their pyrolysis products

	MS	MS300	MS500	MS700	IS	IS300	IS500	IS700
pH	6.85	7.41	7.93	8.45	6.97	7.68	8.59	9.52
Ash (%)	56.74	64.53	71.4	75.42	64.73	72.03	76.94	81.43
C (%)	23.69	19.75	16.23	14.06	19.86	17.72	15.09	12.26
H (%)	1.96	1.34	0.86	0.72	1.43	0.95	0.67	0.51
O (%)	11.53	9.94	8.26	6.88	9.56	5.62	4.12	3.51
N (%)	3.72	2.59	2.04	1.85	2.56	2.04	1.73	1.43
S (%)	2.36	1.85	1.21	1.07	1.86	1.64	1.45	0.86
H/C	0.072	0.054	0.044	0.042	0.083	0.068	0.053	0.051
SSA ($m^2\ g^{-1}$)	12.87	57.91	89.24	105.34	5.69	23.07	34.73	48.46
PV ($cm^3\ g^{-1}$)	0.023	0.094	0.238	0.371	0.008	0.016	0.084	0.103
PD (nm)	6.74	12.92	6.34	3.61	9.35	10.49	8.62	5.40

linked to more vigorous organic decomposition–condensation reactions in MS, while IS's ash content may had inhibited micropore formation.[2,17]

3.1.4 FTIR and XRD analysis. Based on FTIR analysis (Fig. 2a and b), all biochars exhibited a broad peak at 3430 cm^{-1} attributed to –OH stretching vibrations, which diminished with rising pyrolysis temperature, indicating decomposition of hydroxyl groups (–OH) associated with water, alcohols, and carboxylic acids.[3] The peak at ~2922 cm^{-1}, assigned to –CH_2 stretching vibrations, confirmed aliphatic carbon structures. This peak disappeared at ≥500 °C, demonstrating the decomposition of aliphatic hydrocarbons into gases (*e.g.*, CO_2, methyl hydrides) or their conversion to aromatic structures.[17] The C=O

stretching vibration peak at 1656 cm^{-1} shifted to 1620 cm^{-1} at 700 °C, suggesting potential complexation between C=O and heavy metals.[6] The C–O stretching vibration peak at 1421 cm^{-1} gradually weakened with temperature.[22] The peak at 1040 cm^{-1} corresponded to C–O or Si–O stretching vibrations, consistent with high silica content in raw sludge.[16,21] Aromatic C–H bending vibrations at 782 cm^{-1} and 695 cm^{-1} intensified at higher temperatures, confirming the formation of aromatic ring structures.[9] Peaks at 470 cm^{-1} and 530 cm^{-1} were assigned to Al–O–Si bending vibrations, which may react with heavy metals to form silicate precipitates, enhancing stabilization.[9]

XRD analysis (Fig. 2c and d) identified SiO_2 (PDF#46-1045) and gismondine (PDF#20-0452) as the primary crystalline
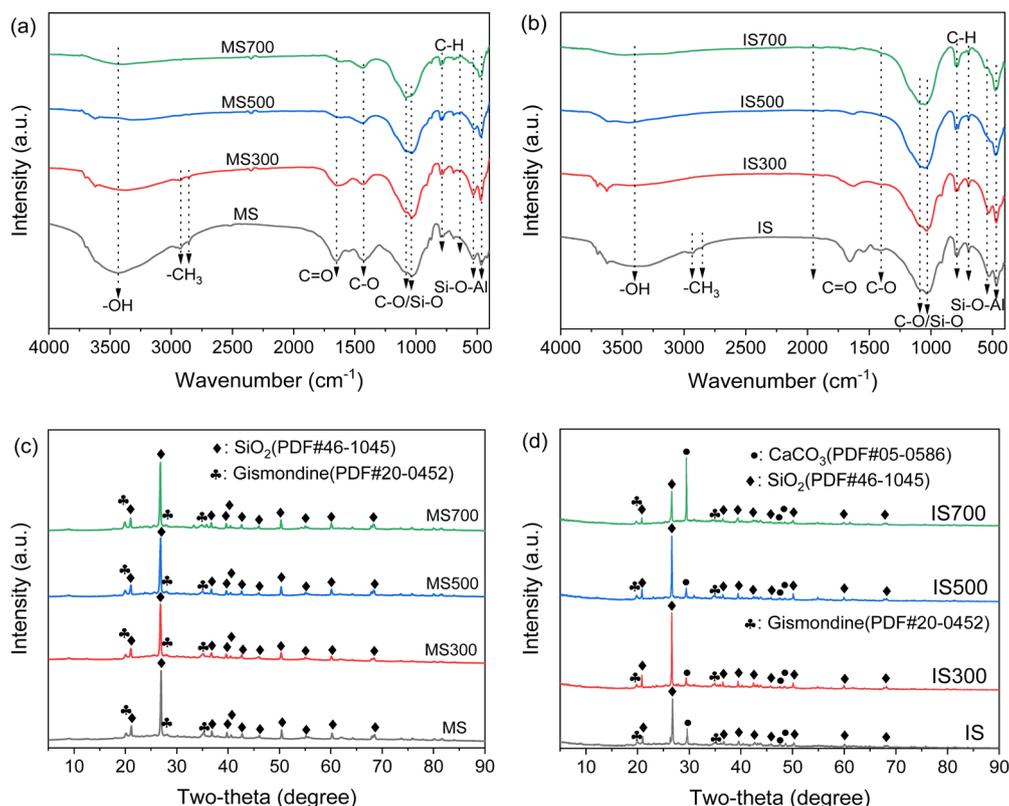

Fig. 2 FTIR ((a) MS and (b) IS) and XRD ((c) MS and (d) IS) analysis of different types of sludge and their pyrolysis products.
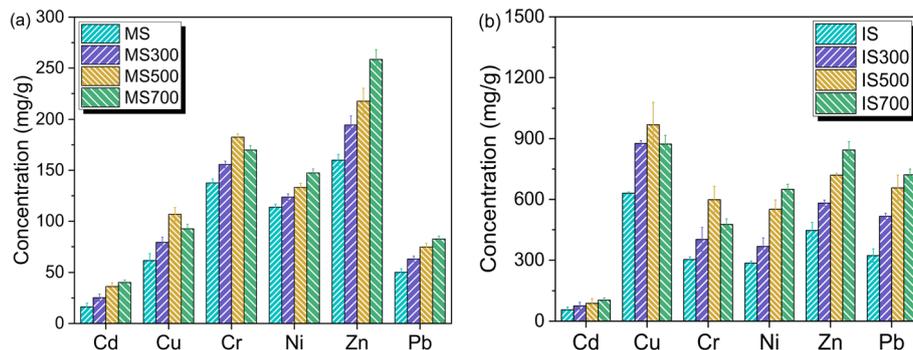
Fig. 3 Analysis of heavy metal content in sludge at different pyrolysis temperatures ((a) MS and (b) IS).

minerals in both sludge types and pyrolysis products.[2,22] Notably, CaCO$_3$ (PDF#05-0586) was detected in IS-derived samples, further evidencing its higher inorganic content.[9,18]

3.2 Analysis of heavy metals in sludge and pyrolysis products

3.2.1 Heavy metal content analysis. In MS (Fig. 3a), the total heavy metal content followed the order Cd > Cu > Cr > Ni > Zn > Pb, with Zn exhibiting a considerably higher concentration (159.98 mg kg^{-1}), likely due to the widespread use of galvanized pipes in China's municipal drainage systems. In IS (Fig. 3b), the order was Cu > Pb > Zn > Ni > Pb > Cd, with concentrations substantially higher than those in MS. As pyrolysis temperature increased, the total content of Cd, Ni, Zn, and Pb in pyrolysis products showed an upward trend, primarily because the volatilization of water and organic matter at higher temperatures resulted in the relative enrichment of heavy metals in the ash fraction.[23] In contrast, Cr and Cu exhibited an initial increase followed by a decrease, peaking at 500 °C, likely due to the volatilization of heavy metals with pyrolysis gases under high-temperature conditions.[17] In MS, Zn was the most abundant metal, reaching a maximum of 258.54 mg kg^{-1} at 700 °C. In IS, Cu reached its highest concentration (969.01 mg kg^{-1}) at 500 °C. Notably, the total amount of heavy metals in the pyrolysis product may be higher than that in the original sludge, likely due to the enrichment of heavy metals in the residue as a result of organic matter volatilization.[9,16]

3.2.2 Heavy metal speciation analysis. The chemical speciation of heavy metals represents the most critical factor controlling bioavailability and ecotoxicity. In MS (Fig. 4a) and IS (Fig. 4b), the bioavailable fractions (F1 + F2) of heavy metal accounted for 15–55% and 20–78%, respectively, indicating potential environmental risks in raw sludge. During pyrolysis, the proportion of stable fractions (F3 + F4) for Cd, Cu, Cr, Ni, Zn, and Pb increased to varying degrees, suggesting reduced environmental risks in pyrolysis production.[13] In MS, the F4 of Cd, Cr, Zn, and Pb increased with temperature, while Ni's residual fraction decreased, indicating its transformation from stable to unstable forms under high temperatures. Cu's residual fraction remained nearly unchanged, but oxidizable fraction (F3) increased from 37.28% to 45.53%. Similarly, the F3 fractions of Ni and Zn also rose with temperature, possibly due to the decomposition of Fe/Mn oxides (F4 fraction) into oxidizable

forms under high temperatures. Compared to F4, F3 is less stable and may readily convert to bioavailable forms under oxidizing conditions.[3,24] In IS pyrolysis products, the residual fractions of Cd, Cr, Zn, and Pb increased with temperature, indicating their transformation from unstable to stable forms, favoring immobilization. For Cu, the bioavailable fraction (F1 + F2) decreased, while F3 increased, and F4 initially rose before stabilizing, suggesting Cu's conversion from bioavailable to oxidizable forms. Ni exhibited a similar speciation trend to MS.[21,23]

Combined with FTIR results (Fig. 2), heavy metals not only complexed with functional groups (–OH, C–O, C=O) on biochar surfaces but also interacted with π-electrons from aromatic groups to enhance stabilization.[22] However, MS and pyrolysis products contained higher N and O functional groups than IS, implying that π-electron interactions and functional group complexation were not the dominant mechanisms for increased stable fractions of Cd, Cr, Pb, and Zn.[15] Previous research suggested that the rise in stable fractions correlates with increased biochar surface area and pore structure.[9] In this study, the significant enhancement of surface area and pore volume with temperature highlights surface adsorption and pore-filling as the primary stabilization mechanisms. Except for Cu and Ni, the F4 fraction of heavy metals increased with pyrolysis temperature, demonstrating the potential of co-pyrolysis to directly convert unstable fractions into safer residual forms.[9,23] In contrast, Ni's stable fraction decreased with temperature, indicating that low-temperature pyrolysis was more effective for Ni stabilization. FTIR and elemental analysis revealed declining N and O content with temperature, suggesting functional group complexation as the key mechanism for Ni stabilization in biochar.[3,17]

In summary, high-temperature pyrolysis significantly reduced the proportion of unstable heavy metal fractions, passivating their environmental risks. Mineral phase transformations, π-electron interactions, functional group complexation, surface adsorption, and pore-filling collectively enhanced heavy metal stabilization. For Cd, Cu, Cr, Pb, and Zn, surface adsorption and pore-filling driven by increased surface area and porosity dominated stabilization, while N/O functional group complexation primarily contributed to Ni stabilization at low temperatures.
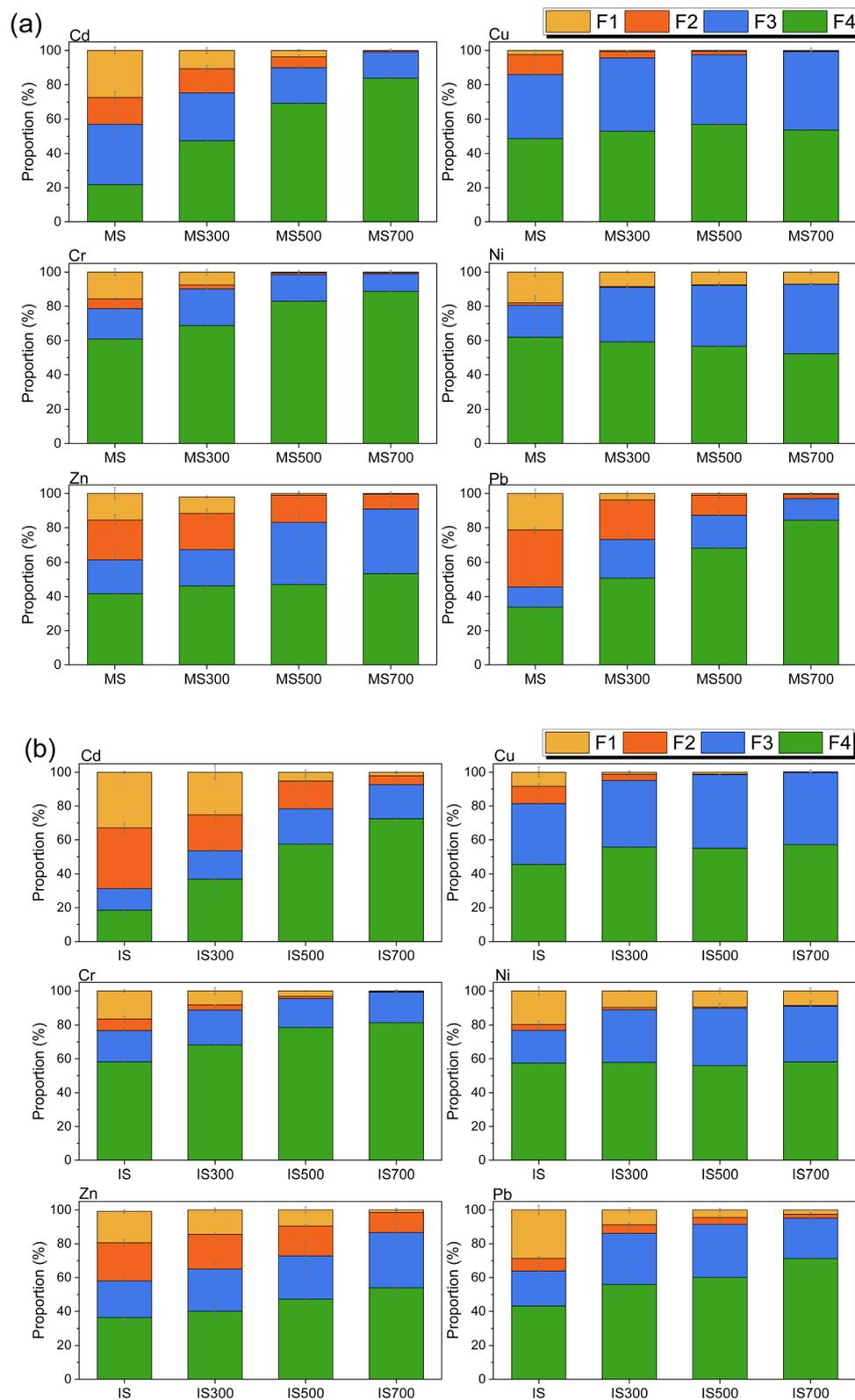
Fig. 4 Morphological analysis of heavy metals in sludge at different pyrolysis temperatures ((a): MS and (b): IS).

3.2.3 Heavy metal leaching analysis. As shown in Table 3, the leaching concentrations of heavy metals generally decreased after pyrolysis in both MS and IS, though variations existed among metals and temperatures. For MS, higher pyrolysis temperatures reduced leaching concentrations of Cd, Cr, Zn, and Pb, but Ni rebounded to 0.225 mg L^{-1} at 700 °C. Cu's

Table 3 Analysis of the concentration of heavy metals in and out of sludge at different pyrolysis temperatures

	Cd	Cu	Cr	Ni	Zn	Pb
MS	0.771	1.649	0.206	0.774	1.533	0.615
MS300	0.447	1.186	0.094	0.257	0.388	0.169
MS500	0.216	1.405	0.041	0.088	0.27	0.081
MS700	0.111	0.949	0.015	0.225	0.104	0.017
IS	2.540	2.542	1.222	3.472	4.132	1.553
IS300	1.870	1.816	0.162	2.847	3.267	0.484
IS500	0.757	1.445	0.068	1.983	2.015	0.246
IS700	0.339	0.935	0.014	1.126	1.856	0.063
China's identification standards for hazardous wastes—toxicity characteristic leaching procedure (GB 5085.3-2007)	1	100	10	5	100	5
U.S. EPA threshold	1	15	5	5	5	5

leaching concentration fluctuated, initially decreasing, then increasing, and finally decreasing again. However, all values for MS and its pyrolysis products remained below the limits set by China's Identification Standards for Hazardous Wastes—Toxicity Characteristic Leaching Procedure (GB 5085.3-2007) and the U.S. EPA threshold (Method 1311, 1990). In IS, leaching concentrations of Cd, Cu, Cr, Ni, Zn, and Pb declined with rising temperature, consistent with prior findings. Notably, the leaching concentration of Cd in IS exceeded 1 mg L^{-1} but dropped to 0.339 mg L^{-1} after high-temperature pyrolysis.

3.3 Risk assessment of heavy metal

3.3.1 Risk assessment code method. According to the tabulated data, the pollution risks of heavy metals in both MS and IS were significantly reduced after pyrolysis treatment, though variations were observed among different metals and sludge types. For MS (Table 4), as the pyrolysis temperature increased from ambient to 700 °C, the RAC value of Cd dropped sharply from 27.35 (medium risk, MR) to 0.15 (no risk, NR), shifting its pollution level from "moderately high" to "non-polluting," demonstrating the excellent stabilization effect of high temperatures on Cd. Similarly, the RAC values of Cr, Zn, and Pb also decreased substantially with rising temperature, with their risk categories all downgraded to NR or low risk (LR). However, Ni in MS700 retained an RAC value of 7.06 (LR),

indicating its relatively poor thermal stability. In IS, the initial RAC value of Cd was notably high (32.94, MR) but decreased to 2.11 (LR) after 700 °C, though some residual risk remained. The RAC value of Zn in IS700 improved significantly to 1.51 (LR) compared to its original value of 18.59 (MR) in IS. However, Ni exhibited the highest residual risk among all metals, with its RAC value only declining from 19.74 to 8.65 (LR) under high-temperature conditions. Notably, Cu performed exceptionally well in both sludge types, with its RAC values reduced to NR or LR at high temperatures, effectively eliminating pollution risks.[2,9,18]

3.3.2 Potential ecological risk index method. The contamination factors (C_f), ecological risk factors (E_r), and risk indices (R_I) of heavy metals in sludge and biochar were shown in Fig. 5. According to the ecological risk assessment criteria (Table S1), the environmental risk levels of heavy metals in sludge and biochar were determined. In MS and IS, the C_f values (Fig. 5a) of Cd were 3.61 and 4.39, respectively, indicating high contamination levels. The C_f values of Cu, Zn, and Pb ranged between 1–3, suggesting low contamination levels in both MS and IS, while Cr and Ni were classified as clean.[25] With increasing pyrolysis temperature, the C_f values of Cd, Cu, Cr, Pb, and Zn gradually decreased, demonstrating that pyrolysis effectively reduced the risk levels of most heavy metals in sludge. However, the C_f value of Ni in MS increased with pyrolysis temperature, whereas in IS, it initially increased before decreasing. At 700 °C, the C_f values of all heavy metals in both MS and IS were below 1, reaching clean levels. Previous studies had shown that the high Zn content in raw sludge makes it difficult to reduce its risk level to clean, highlighting the effectiveness of high-temperature pyrolysis in mitigating heavy metal environmental risks.[9,21,22]

The E_r values (Fig. 5b) of Cd in both raw sludges were at high ecological risk levels, with IS exhibiting higher values than MS. Most pyrolysis products showed E_r values for Cd below 40, indicating low ecological risk, except for IS300, which ranged between 40–80 (moderate risk). For other heavy metals, both raw sludge and pyrolysis products had E_r values below 40, corresponding to low ecological risk. The R_I values (Fig. 5c) of MS and IS peaked at 129.80 and 151.81, respectively, but decreased significantly with increasing pyrolysis temperature, indicating a substantial reduction in potential ecological risks. This confirmed that high-temperature pyrolysis effectively lowered the ecological risk levels of both municipal and industrial sludge.

Table 4 Risk assessment code for sludge at different pyrolysis temperatures

|	Cd		Cu		Cr		Ni		Zn		Pb	
	RAC	Level	RAC	Level	RAC	Level	RAC	Level	RAC	Level	RAC	Level
MS	27.35	MR	2.42	LR	15.68	MR	17.91	MR	15.53	MR	21.35	MR
MS300	10.73	MR	0.72	NR	7.52	LR	8.46	LR	9.65	LR	3.78	LR
MS500	3.71	LR	0.50	NR	0.52	NR	7.45	LR	0.94	NR	0.92	NR
MS700	0.15	NR	0.19	NR	0.32	NR	7.06	LR	0.36	NR	0.59	NR
IS	32.94	MR	8.31	LR	16.41	MR	19.74	MR	18.59	MR	28.69	MR
IS300	21.19	MR	1.24	LR	8.21	LR	9.69	LR	14.48	MR	8.80	LR
IS500	5.29	LR	1.15	LR	3.15	LR	9.45	LR	9.63	LR	4.44	LR
IS700	2.11	LR	0.32	NR	0.40	NR	8.65	LR	1.51	LR	2.60	LR
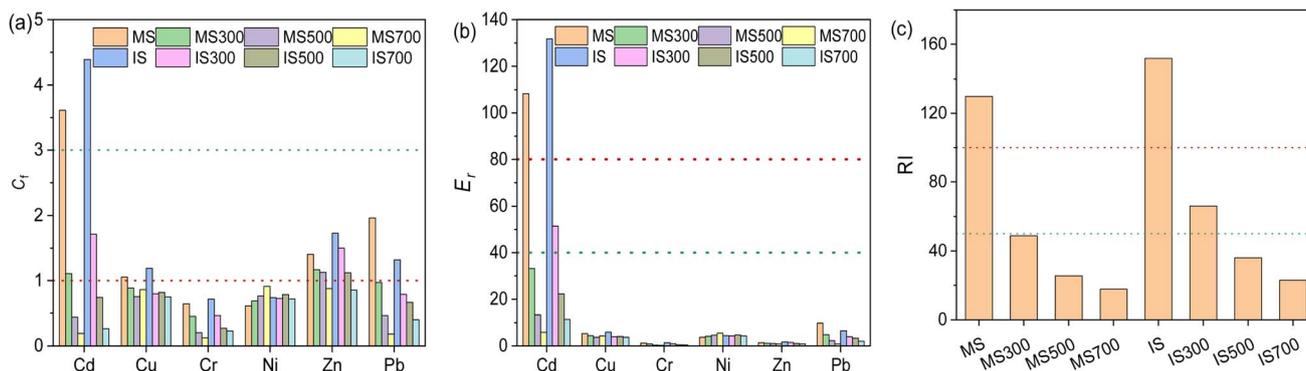
Fig. 5 Evaluation of heavy metal ecological risk of sludge species at different pyrolysis temperatures ((a): C_f, (b): E_r and (c): R_I).

4 Conclusions

This study elucidated the regulatory mechanisms of pyrolysis temperature (300–700 °C) on the speciation transformation and environmental risks of heavy metals in biochar derived from MS and IS. High-temperature pyrolysis (700 °C) enhanced the stabilization of Cd, Cr, Pb, and Zn by increasing biochar's specific surface area and pore structure, with surface adsorption and pore-filling as the dominant mechanisms. In contrast, the stabilization of Cu and Ni at low pyrolysis temperatures (300–500 °C) primarily relied on complexation with N/O-containing functional groups. After pyrolysis, the proportions of bioavailable heavy metal fractions and leaching concentrations decreased, while the potential ecological risk index was reduced compared to raw sludge. These findings provided theoretical and technical foundations for the safe disposal of sludge.

Author contributions

Ke Zhao: investigation, data analysis, methodology, software, supervision, writing – original draft, review & editing; Chundi Si: investigation, methodology, supervision, funding, review & editing; Pei Zhang: review & editing; Yaning Cui: review & editing.

Conflicts of interest

The authors declare that they have no known competing financial interests or personal relationships that could have appeared to influence the work reported in this paper.

Data availability

Data will be made available on request. Supplementary information: heavy metal risk assessment methods (risk assessment index and potential ecological risk index), as well as Table S1: Classification of potential ecological risk levels. See DOI: **https://doi.org/10.1039/d5ra04990c**.

Acknowledgements

References

1 Y. X. Yang, Z. P. Zhong, B. S. Jin, B. Zhang, H. R. Du, Q. Li, X. Zheng, R. Z. Qi, P. K. Ren and Z. Y. Li, *Waste Manage.*, 2024, **178**, 126–134.

2 S. H. Deng, K. Xu, Z. Xia, S. L. Yu, X. B. Wang, H. Z. Tan and R. H. Ruan, *J. Environ. Chem. Eng.*, 2025, **13**, 115638.

3 Y. Liu, A. Ali Siyal, C. B. Zhou, C. L. Liu, J. Fu, Y. W. Zhang, B. Yao, L. Chao, H. M. Yun, J. J. Dai and X. T. Bi, *Chem. Eng. J.*, 2024, **485**, 150032.

4 X. J. Zhou, X. L. Guo, L. L. Liu, H. D. Zhai, Q. G. Meng, Z. Shi and X. S. Tai, *RSC Adv.*, 2020, **10**, 4817–4824.

5 M. F. Liu, K. Q. Wang, H. L. Wang, J. Lu, S. K. Xu, L. L. Zhao, X. L. Wang and J. M. Du, *RSC Adv.*, 2021, **11**, 11732–11738.

6 A. Zhou, S. L. Yu, S. H. Deng, H. Mikulčić, H. Z. Tan and X. B. Wang, *J. Energy Inst.*, 2023, **111**, 101417.

7 Z. J. Li, H. Deng, L. Yang, G. L. Zhang, Y. Q. Li and Y. S. Ren, *Bioresour. Technol.*, 2018, **256**, 216–223.

8 C. X. Li, J. Li, S. Y. Xie, G. Y. Zhang, L. J. Pan, R. M. Wang, G. Wang, X. F. Pan, Y. Wang and I. Angelidaki, *J. Clean. Prod.*, 2022, **369**, 133325.

9 J. W. Jin, Y. N. Li, J. Y. Zhang, S. C. Wu, Y. C. Cao, P. Liang, J. Zhang, M. H. Wong, M. Y. Wang, S. D. Shan and P. Christie, *J. Hazard. Mater.*, 2016, **320**, 417–426.

10 Z. L. Sun, Z. S. Chen, X. S. Tai and X. K. Wang, *Sci. China Chem.*, 2025, **68**, 3923–3926.

11 W. H. Gu, J. S. Guo, J. F. Bai, B. Dong, J. Hu, X. N. Zhuang, C. L. Zhang and K. Shih, *J. Environ. Manage.*, 2022, **305**, 114292.

12 G. H. Mo, J. Xiao and X. Gao, *Environ. Sci. Pollut. Res.*, 2023, **30**, 57771–57787.

13 L. L. Wang, H. F. Tu, H. H. Zhang, L. C. Liang, H. Jiang, D. Wang, X. F. Yan and Y. S. Xu, *Waste Manage.*, 2024, **183**, 174–183.

14 P. Devi and A. K. Saroha, *Bioresour. Technol.*, 2014, **162**, 308–315.

15 M. Y. Lv, T. T. Zhao, J. J. Chen, L. Z. Tong, Z. B. Ni, Q. Q. Lin, Z. P. Ruan and R. L. Qiu, *Environ. Technol. Inno.*, 2025, **37**, 104049.

16 T. M. Embaye, A. Zhou, R. Li, M. B. Ahmed, R. H. Ruan, D. Y. Wu, N. Deng and X. B. Wang, *Process Safe. Environ.*, 2025, **193**, 1332–1342.

17 M. Z. Li, Y. J. Hu, N. Zhou, S. R. Wang and F. F. Sun, *J. Hazard. Mater.*, 2022, **438**, 129539.

18 X. Min, T. Ge, H. Li, Y. H. Shi, T. Fang, B. X. Sheng, H. Y. Li and X. J. Dong, *Chemosphere*, 2022, **290**, 133371.

19 A. Yadav, P. Yadav, S. Bojjagani, J. K. Srivastava and A. Raj, *Chemosphere*, 2024, **360**, 142454.

20 Y. X. Yang, Z. P. Zhong, Z. A. Zhen, B. S. Jin, B. Zhang, H. R. Du, Q. Li, X. Zheng, R. Z. Qi, Q. H. Ye and Y. Jia, *J. Anal. Appl. Pyrol.*, 2024, **182**, 106725.

21 Q. Li, Z. P. Zhong, H. R. Du, Y. X. Yang, X. Zheng and R. Z. Qi, *J. Anal. Appl. Pyrol.*, 2024, **181**, 106595.

22 G. Y. Xu, X. X. Yang, F. H. Yu, J. N. Mei, M. M. Liu, M. S. Li, T. Zhu and B. Z. Fang, *Sci. Total Environ.*, 2024, **951**, 175653.

23 J. Shen, Y. Wu, G. X. Lan, Y. P. Xia, B. Yan, Y. R. Li, Y. X. Zhang, Y. Yu, C. Fu, A. J. Xu, J. Zhou, A. L. Zhu and D. Chen, *J. Environ. Chem.Eng.*, 2023, **11**, 110406.

24 X. Y. Chang, P. F. Wu, Y. Z. Chu, Y. Zhou and Y. Y. Tang, *Waste Manage.*, 2024, **189**, 401–409.

25 L. J. Bai, B. Wu, J. L. Cao and X. H. Dai, *J. Anal. Appl. Pyrol.*, 2025, **190**, 107137.